Laser fluorescence detection of nascent product state distributions in reactions of Sc and Y with O2, NO, and SO2

K. Liu and J. M. Parson

Citation: The Journal of Chemical Physics **67**, 1814 (1977); doi: 10.1063/1.435138
View online: http://dx.doi.org/10.1063/1.435138
View Table of Contents: http://scitation.aip.org/content/aip/journal/jcp/67/5?ver=pdfcov
Published by the AIP Publishing

Laser fluorescence detection of nascent product state distributions in reactions of Sc and Y with O_2, NO, and SO_2

K. Liu and J. M. Parson[a)]

Chemistry Department, The Ohio State University, Columbus, Ohio 43210
(Received 18 May 1977)

The reactions of Y and Sc with O_2, NO, and SO_2 have been investigated by the laser-induced fluorescence method. The excitation spectra are reported for metal oxide products formed under single-collision conditions in a beam–gas arrangement. Possible systematic errors which arise in deducing the internal state distributions from the spectra are discussed. The relative vibrational populations of metal oxides for all reactions are close to unbiased statistical distributions (in the sense of the information theoretic approach). Although the rotational distributions from the reactions with NO and SO_2 also follow statistical behavior, those from the reactions with O_2 peak significantly lower than the statistical ones. Radiative lifetimes are reported for the *A* and *B* states of YO and ScO, and the *B* and *C* states of LaO.

I. INTRODUCTION

A wealth of chemical dynamic information has been provided by applications of the laser-induced fluorescence technique[1] to molecular beam chemistry since 1972. The advantages of this method for the study of beam reactions are high detection efficiency, narrow laser bandwidths allowing the simultaneous determination of both vibrational and rotational distributions,[2] and the possibility of measuring several even more detailed features in chemical reactions.[3]

The production of electronically excited metal oxides in the oxidation reactions of Group IIIB atoms has been studied extensively previously.[4,5,6] One striking feature of those investigations is that both the initial translational energy dependence and vibrational energy disposal are close to prior predictions based solely on product state densities. Since ground electronic state molecules are expected to comprise most of the reaction products, it is essential to characterize their energy distributions before making any general conclusions about the dynamics of Group IIIB atom oxidation reactions.

We report here the internal energy distributions of the YO (ScO) products formed by Y(Sc) + O_2, NO, and SO_2 reactions under single-collision conditions. These distributions are determined from laser-induced fluorescence excitation spectra. Here, a tunable narrow-band light source (nitrogen pumped dye laser) is swept in wavelength. When it coincides with a molecular absorption line the molecule is excited to an electronically excited state and is detected by observing the subsequent undispersed light emission of the molecule.

The experimental observations then serve as a sensitive test of the applicability of statistical models to these systems.

II. EXPERIMENTAL

The experimental arrangement consists of a molecular beam apparatus, a pulsed tunable dye laser, a gated optical detection system, and an on-line computer. The molecular beam system has been described in detail previously[4] except for the metal beam source, which was a new design. The metal was evaporated from a cylindrical tungsten oven (2.8 cm diam. × 3.2 cm height) containing a replaceable tungsten crucible and having a 3 mm diam. beam orifice. The oven was heated by passing a high ac current through a tungsten mesh radiator (GTE Sylvania) which was surrounded by either tungsten or molybdenum radiation shields or a graphite felt radiation shield (Union Carbide). The oven temperature was measured with a calibrated optical pyrometer focussed on the back of the oven behind the beam orifice. Based on available data[7] the vapor pressure of Y in the oven was about 0.1 torr at the operation temperature of 2100 K, and that of Sc was 0.2 torr at 1850 K. The metal beam was collimated by a series of holes in the radiation shields and in a water-cooled copper jacket, and by a 3 mm high × 2 mm wide slit before flying into the (separately pumped) reaction chamber. The distance between the slit and the laser excitation zone was 3 cm.

The reaction chamber was filled with an oxidant gas which was leaked through a needle valve to a location remote from the laser excitation zone to assure an accurately known and constant pressure at the laser excitation zone (typically $1-2 \times 10^{-4}$ torr). The pressure was measured with a capacitance nanometer (Datametrics) located near the laser excitation zone.

An appreciable YO induced-fluorescence signal (see below) was found to occur even without any oxidant gas present, apparently due to thermal decomposition of Y_2O_3 impurity in the Y sample. To avoid having to make large corrections for this thermal signal in the reactively formed YO signal the Y sample was preheated with NH_4Cl, which converts Y_2O_3 to the more volatile YCl_3. No interference from new molecular species occurred with this treatment of the Y sample, and the percentage of the signal due to thermal YO was reduced to less than 10% at all wavelengths. In the case of Sc the thermal ScO signal was smaller than the thermal YO signal without any treatment (negligible with one Sc sample and less than 25% of total signal with another),

[a)]Alfred P. Sloan Foundation Fellow.

and the procedure followed to remove Y_2O_3 did not help to reduce the Sc_2O_3 further.

The laser used was a pulsed dye laser (Reich Associates) of the Hänsch type,[8] pumped by 100 kW peak power nitrogen laser (Avco model 5000) at 200 pps. A dye laser bandwidth of 0.3–0.4 Å was obtained using a beam expander (Molectron) and an 1800 lines/mm grating in first order. A stepping motor was used to drive the grating. The dyes used were Rhodamine B (5×10^{-3} M in ethanol) for exciting the $X^2\Sigma$–$A^2\Pi$ transition of YO or ScO or Coumarin 102 (5×10^{-3} M in ethanol) for exciting the $X^2\Sigma$–$B^2\Sigma$ transition of YO or ScO. A laser energy of typically 2×10^{-5} J per pulse was measured by a joulemeter (Molectron). The output laser beam passed through a beam splitter, a set of neutral density filters (with a reduction factor of typically 1/10 to avoid saturation of the transitions), an adjustable diaphragm, and a series of pinholes before being sent into the reaction chamber. A broad band antireflection-coated entrance prism and exit window for the laser beam were located at the beginning and end, respectively, of carefully positioned blackened light baffles. The laser intensity reflected from the beam splitter was monitored by either a PM tube (RCA 1P28) or a photodiode (EEG model SGD-040). Its output was then fed into a boxcar integrator (Channel B, PAR model 164) for further processing. The YO or ScO induced fluorescence was observed by a water-cooled PM tube (EMI 9816B) which was mounted inside the collision chamber with the viewing direction perpendicular to the laser and metal beams. A carefully designed spatial filter was housed in front of the PM tube to eliminate background photons originating from scattered laser light and the dc signal from the hot metal beam source. The PM tube signal was fed into the boxcar integrator (Channel A, PAR model 164). The gate of the integrator was opened a few nanoseconds before the arrival of the fluorescence signal and kept open for 100 ns, which is approximately three times the radiative lifetimes of the ScO and YO excited states (see below). The gated signal A/B was then amplified and exponentially averaged over typically 800 successive laser pulses. The resultant output was transferred through a DVM (Fluke 8200 A) into a computer (Hewlett Packard 9830) for storing the data and plotting the normalized fluorescence signal. Then the computer stepped the laser to the next wavelength.

Periodic corrections for background drift were made by closing the metal beam flag and subtracting the interpolated background signal at every data point. Corrections for drift in the metal beam intensity and for long term variations of detector efficiency were made by measuring either a fluorescence peak intensity at the beginning and end of a scan, or in some cases the total chemiluminescence intensity. The latter was monitored periodically by using an ammeter (Keithley 427). Both methods gave reasonably consistent results. For the reaction with O_2 interference from the large chemiluminescent dc signal necessitated operation at a lower gas pressure and oven temperature, and a slightly stronger laser intensity for the reaction with Y. Due to the weaker fluorescence signal in the case of the $Sc+O_2$ reaction a full-powered laser was employed. The Appendix describes how the signal in this partially saturated case was analyzed. Finally, the spectral responses of both PM tubes and the photodiode were determined by comparing the responses to that of a joulemeter (Molectron).

III. RESULTS

A. Radiative lifetimes

The radiative lifetimes of electronically excited molecules have gained considerable attention because of their role in understanding the nature of electronic transitions, and also because of their importance in interpreting laser-induced fluorescence and chemiluminescence experiments. Since the Group IIIB monoxides are isolectronic to the alkaline earth monohalides, for which lifetimes are available,[9] one expects lifetimes of the $A^2\Pi$ and $B^2\Sigma$ to be on the order of 20–40 ns. Indeed, this was found, as shown in Table I.

The apparatus used to determine the radiative lifetimes was essentially the same as that employed to measure internal state distributions in the products from chemical reactions. The only change was the use of the boxcar integrator scanning mode with a 5 ns aperture duration. The output of the boxcar integrator was displayed on a stripchart recorder. The fluorescence intensity of a single scan was read off the chart at equally spaced time intervals. Radiative lifetimes were determined from least square analysis of the portion of the trace 30 ns or more after the peak fluorescence intensity (where the time response of the detection system and the finite laser width were no longer

TABLE I. Radiative lifetimes and electronic transition moments for Group IIIB oxides.

Molecule	State		λ_{ex}(Å)	τ(ns)[a]	R_e^2(a.u.)[b]
ScO	$A^2\Pi_{1/2}$,	$v=0$	6079.3	35.9±2.4	3.09±0.21
	$A^2\Pi_{3/2}$,	$v=0$	6036.2	27.0±2.5	2.93±0.21
	$B^2\Sigma$,	$v=0$	4857.8	33.3±0.6	1.70±0.03
YO	$A^2\Pi_{1/2}$,	$v=0$	6132.1	33.0±1.3	3.45±0.15
		$v=1$	6148.4	36.5±2.4	3.14±0.21
	$A^2\Pi_{3/2}$,	$v=0$	5972.0	32.3±0.9	3.25±0.10
		$v=1$	5987.6	30.4±1.8	3.48±0.21
		$v=2$	6003.6	33.4±1.5	3.20±0.15
		$v=6$	6070.6	41.6±2.1	2.65±0.12
	$B^2\Sigma$,	$v=0$	4818.2	30.0±0.9	1.84±0.06
		$v=1$	4842.5	32.5±1.2	1.72±0.06
LaO	$B^2\Sigma$,	$v=0$	5600.0	34.2±1.5	2.53±0.12
			5602.4	35.5±1.2	2.44±0.09
		$v=1$	5626.0	36.0±1.8	2.44±0.12
			5628.6	35.9±2.4	2.72±0.18
	$C^2\Pi_{1/2}$,	$v=0$	4418.2	26.9±0.9	1.58±0.06
	$C^2\Pi_{3/2}$,	$v=0$	4372.0	28.3±1.8	1.46±0.09

[a]The errors cited are three times one standard deviation.
[b]The electronic transition moment is defined by $A_{v'v''}=(64\Pi^4/3h)\nu^3_{v'v''}q_{v'v''}R_e^2$ and $1/\tau_{v'v''}\approx A_{v'v''}$, based on the near unity FC factors.

important in determining the shape of the fluorescence curve). The lifetime of a state was computed as the average of the lifetimes from a number of such scans (typically 4–5 scans). The time base of the detector system was calibrated by a standard crystal oscillator. No wavelength selection of the fluorescence was employed. However, since there is a low-lying excited electronic state $A'^2\Delta$,[5] cascading from $A^2\Pi$ to $A'^2\Delta$, followed by detection of $A'^2-X^2\Sigma$ emission, might possibly lengthen the measured lifetime. A 6500 Å cut-on filter, which would pass only $A'^2\Delta-X^2\Sigma$ emission, was placed in front of the PM tube to test for the likelihood of the process in YO. No emission was detectable with the filter installed, and hence this alternative decay process was unimportant, as would be expected if the transition moment for the $A^2\Pi-A'^2\Delta$ transition is less than or comparable to that for the $A^2\Pi-X^2\Sigma$ transition. The lifetimes were determined using the reaction with SO_2 to form the metal oxides at SO_2 pressures in the low 10^{-5} torr range. Under these conditions systematic errors caused by radiation trapping and electronic quenching were expected to be negligible. Finally, we would like to point out in the results shown in Table I that the electronic transition moments are essentially constant (except for $A^2\Pi_{3/2}$, $v=6$, which is a strongly perturbed level). This fact has been used to simplify the simulation program described below.

B. Excitation spectra

The YO product molecule was detected by using the laser-induced fluorescence of the $X^2\Sigma-A^2\Pi_{1/2,3/2}$ band systems (5970–6360 Å). Figures 1–3 show typical scans of the YO excitation spectra (normalized fluorescence intensity vs laser wavelength) for the reactions studied. Several well resolved peaks are recognized and easily assigned to the $\Delta v=0$ sequence.[10] Indeed, in the Franck–Condon (FC) factors the $\Delta v=0$ sequence comprised over 80% of the total intensity for $0\leq v\leq 7$. The $X^2\Sigma-{}^2\Pi_{3/2}$ (6, 6) and $X^2\Sigma-{}^2\Pi_{1/2}$ (7, 7) transitions are abnormal due to perturbations.

Although the branch structure of a single band in these two electronic transitions are quite similar, the main features of the resultant spectra are dominated by different portions of the rotational distributions due to the slight difference in their spectroscopic constants, particularly the effective rotational constant. For example, the J values at the most prominent heads in the $X-{}^2\Pi_{3/2}$ and $X-{}^2\Pi_{1/2}$ transitions, Q_2 and Q_1 branches, respectively, are 74 and 53. Thus, a simple analysis of the excitation spectra in terms of peak heights would yield different vibrational distributions for the X state depending on which transition was used. The difference in the $X-{}^2\Pi_{3/2}$ and $X-{}^2\Pi_{1/2}$ spectra, though, can be used to advantage if a computer simulation of the spectra is performed. Then the different transitions will give complementary information about the rotational distribution of the X state.

Since a beam–gas arrangement was employed in the present studies, tests were made for possible complications due to collisional relaxation by comparing the excitation spectra taken at different gas pressures. Within the range $0.5-3\times10^{-4}$ torr of SO_2 gas no significant changes were noticed (< 10%). Therefore, we conclude that the excitation spectra shown represent the nascent distributions of the number density of product molecules.

The ScO product molecule was detected under un-

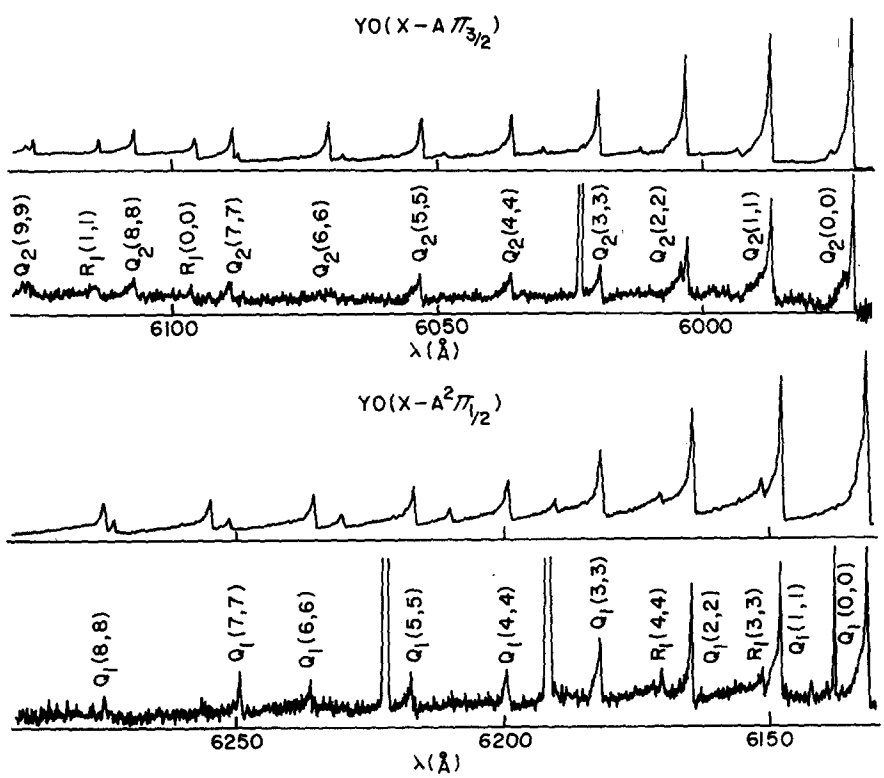

FIG. 1. YO excitation spectrum of the $X^2\Sigma^+-A^2\Pi_{3/2}$ and $X^2\Sigma^+-A^2\Pi_{1/2}$ transitions for the $Y+O_2$ reaction. The upper panels show the simulated spectrum.

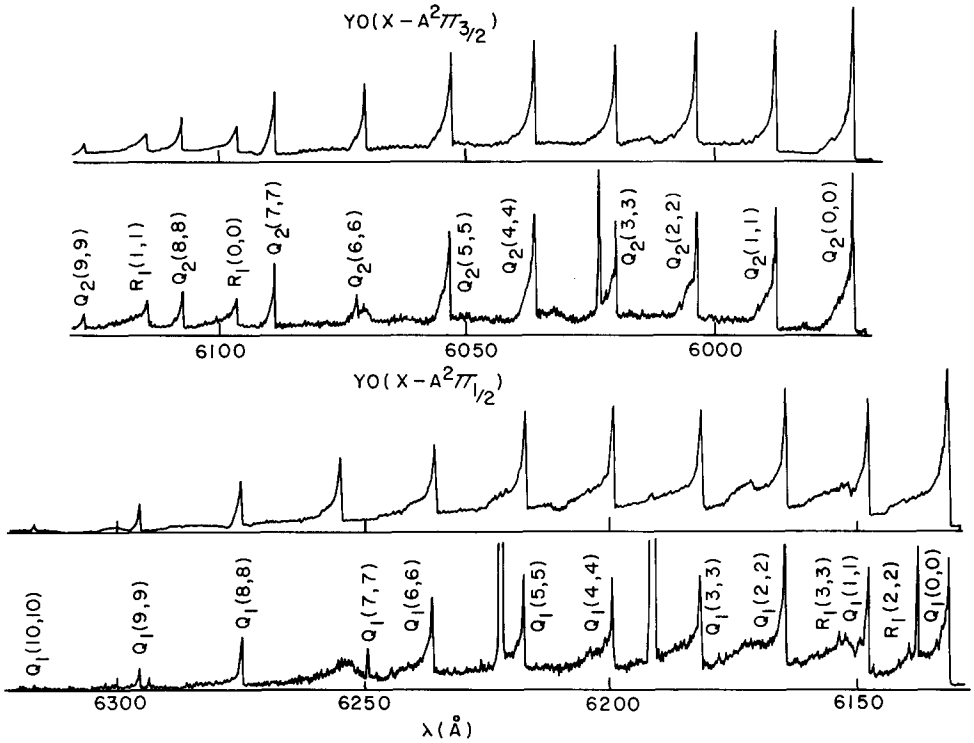

FIG. 2. YO excitation spectrum of the $X^2\Sigma^+$–$A^2\Pi_{3/2}$ and $X^2\Sigma^+$–$A^2\Pi_{1/2}$ transitions for the Y + NO reaction. The upper panels show the simulated spectrum.

saturated conditions using the $X^2\Sigma$–$A^2\Pi_{1/2,3/2}$ systems in the case of reaction with NO and SO_2, and using the $X^2\Sigma$–$B^2\Sigma$ system for reaction with all three gases. Figures 4–8 show scans of the ScO excitation spectra. In the X–A spectra it should be noted that there is extensive overlap between excitation to the $\Pi_{1/2}$ and $\Pi_{3/2}$ states, making separate analysis difficult and requiring computer simulation. In the X–B spectra partially resolved rotational structure is evident, but the overlap of several branches precludes association of the separate peaks with excitation of individual vibrotational states.

C. Computer simulation

The basic principles involved in applications of the laser-induced fluorescence technique to determination of internal state distributions of reaction products have been discussed extensively by Zare and co-workers.[1,3d] The total fluorescence intensity $I_{v'J'}^{v''J''}$ (energy/s) cor-

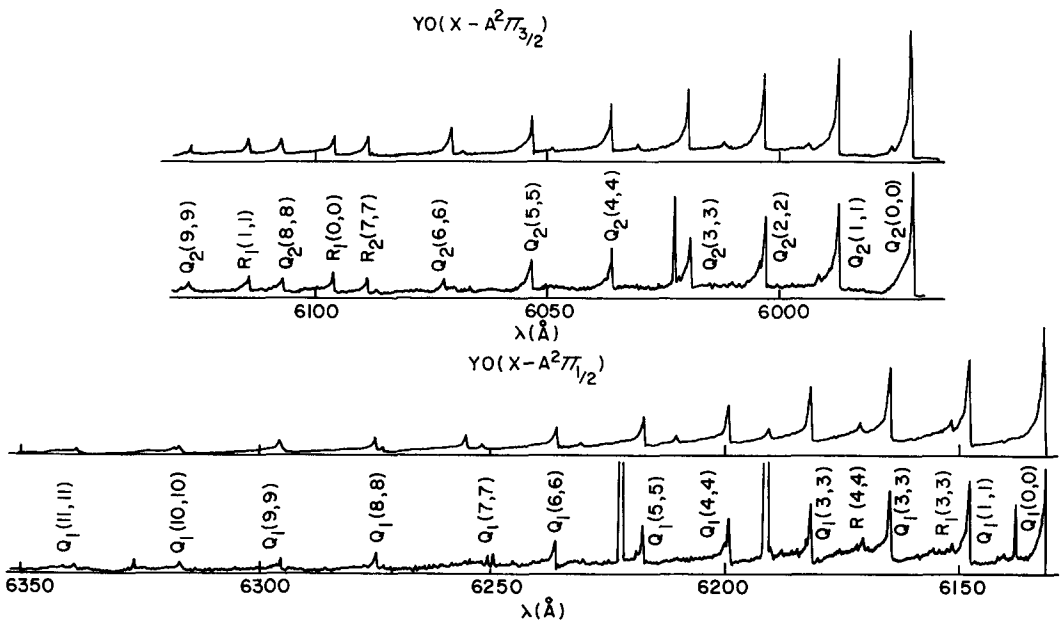

FIG. 3. YO excitation spectrum of the $X^2\Sigma^+$–$A^2\Pi_{3/2}$ and $X^2\Sigma^+$–$A^2\Pi_{1/2}$ transitions for the Y + SO_2 reaction. The upper panels show the simulated spectrum.

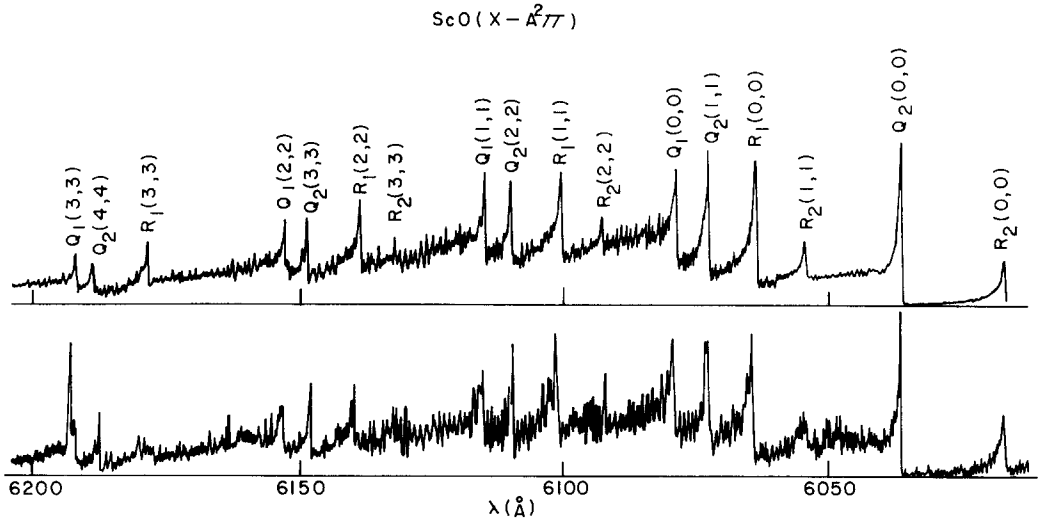

FIG. 4. ScO excitation spectrum of the $X^2\Sigma^+$–$A^2\Pi$ transition for the Sc + NO reaction. The Q_1, R_1 branches indicate the X–$A\,^2\Pi_{1/2}$ transition, and Q_2, R_2 the X–$A\,^2\Pi_{3/2}$ transition. The upper panels show the simulated spectrum.

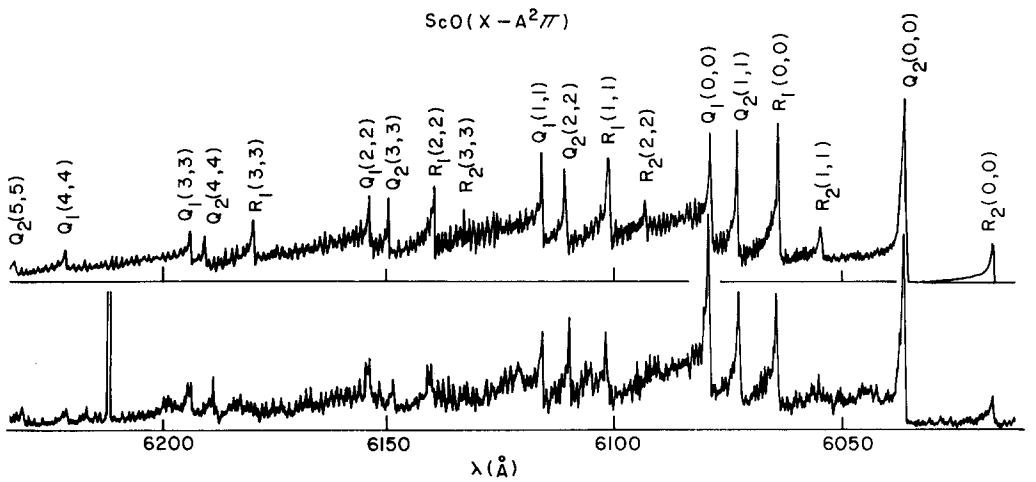

FIG. 5. ScO excitation spectrum of the $X^2\Sigma^+$–$A^2\Pi$ transition for the Sc + SO_2 reaction. The Q_1, R_1 branches indicate the X–$A\,^2\Pi_{1/2}$ transition, and Q_2, R_2 the X–$A\,^2\Pi_{3/2}$ transition. The upper panels show the simulated spectrum.

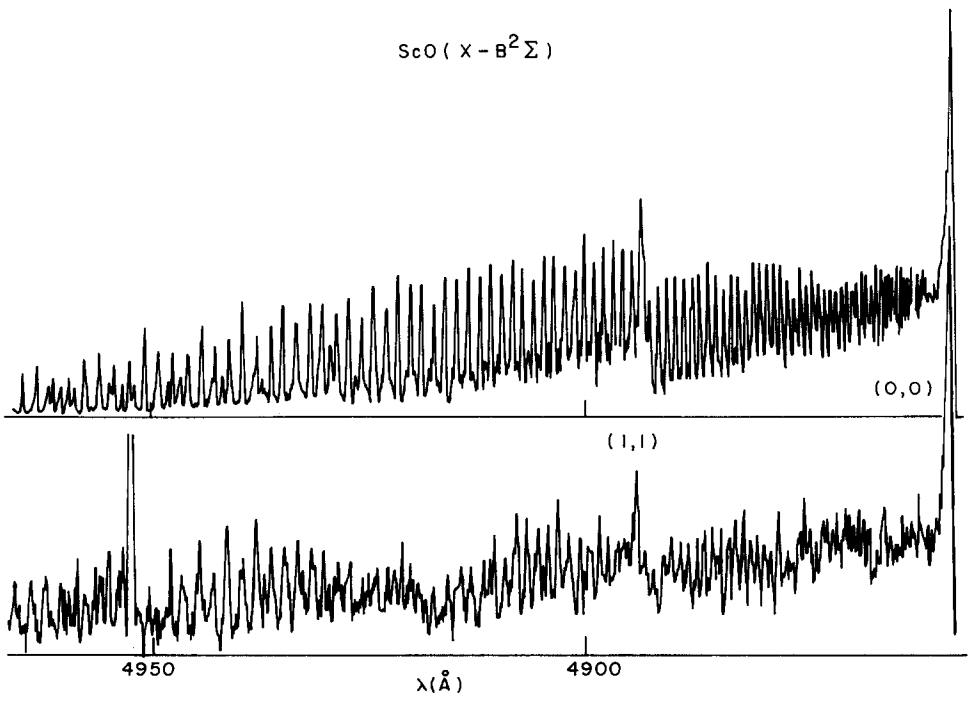

FIG. 6. ScO excitation spectrum of the $X^2\Sigma^+$–$B^2\Sigma$ transition for the Sc + O_2 reaction. The simulated spectrum is shown in the upper panel.

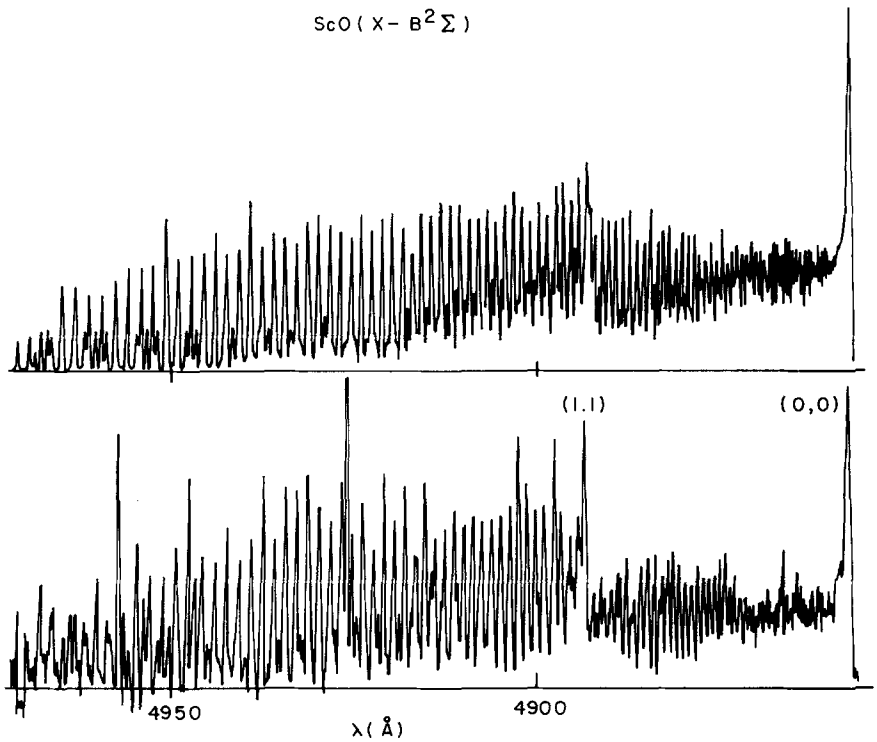

FIG. 7. ScO excitation spectrum of the $X^2\Sigma^+$–$B^2\Sigma$ transition for the Sc + NO reaction. The simulated spectrum is shown in the upper panel.

responding to excitation from the lower (v'', J'') vibrational–rotational level to the upper (v', J') level is given in the Born–Oppenheimer approximation by

$$I_{v''J''}^{v'J'} = k\left[n(v'', J'')\rho(\lambda_{v''J''}^{v'J'}) q_{v'v''} \frac{S_{J'J''}}{(2J''+1)}\right] \times\left[\sum_{v,J} (\nu_{vJ}^{v'J'})^4 q_{v'v} \frac{S_{JJ'}}{(2J'+1)} R(\lambda_{vJ}^{v'J'})\right] \frac{1}{g_{\Lambda''S''}g_{\Lambda'S'}}, \quad (1)$$

where $n(v'', J')$ is the number density of the (v'', J'') level (summed over magnetic sublevels), $\rho(\lambda_{v''J''}^{v'J'})$ is the laser energy density at the wavelength $\lambda_{v''J''}^{v'J'}$ of the transition $v''J'' \rightarrow v'J'$, q and ν are the FC factor and frequency, respectively, for the denoted transition, $S_{J'J''}$ is the rotational line strength for the $J'' \rightarrow J'$ transition, $R(\lambda_{vJ}^{v'J'})$ is the (energy) response of the detector at the wavelength $\lambda_{vJ}^{v'J'}$, the g's are electronic degeneracy factors = $(2S+1)(2-\delta_{0\Lambda})$, and k is a proportionality constant which includes geometric factors, polarization,

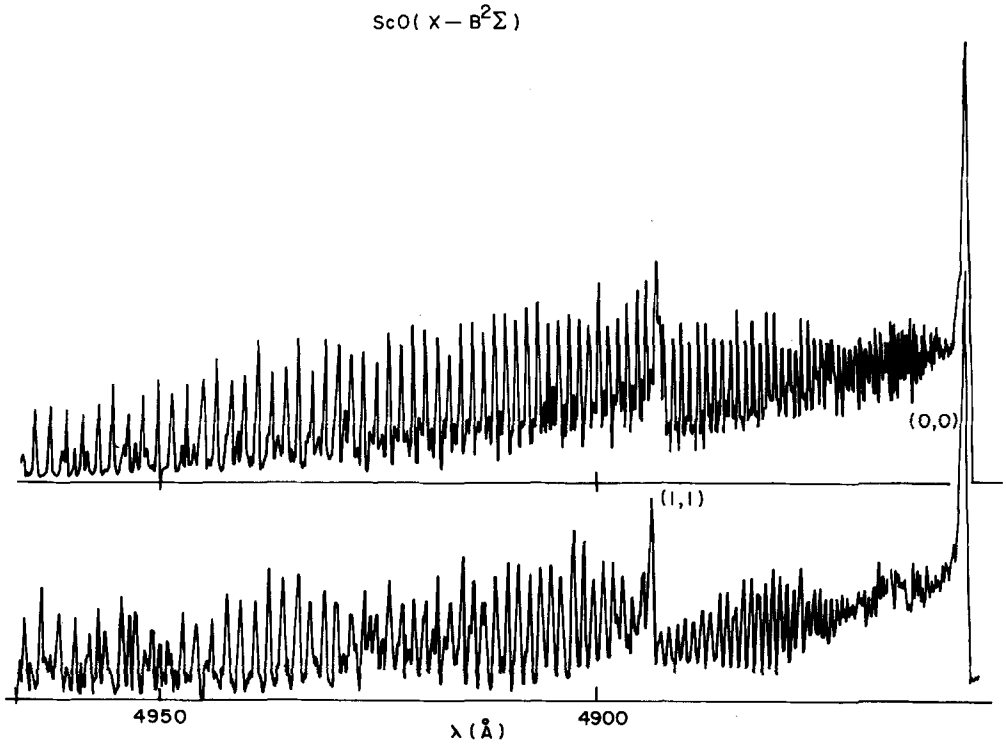

FIG. 8. ScO excitation spectrum of the $X^2\Sigma^+$–$B^2\Sigma$ transition for the Sc + SO_2 reaction. The simulated spectrum is shown in the upper panel.

etc. If the boxcar integrator gate duration is long compared to the upper level radiative lifetime, then the summation over v, J in Eq. (1) should be changed to allow for the fact that essentially all excited molecules radiate in time to be detected.[4] The summation over v, J should be replaced by

$$\sum_{vJ}\left[(\nu_{vJ}^{v'J'})^4 q_{v'v}\frac{S_{J'J''}}{(2J'+1)}R(\lambda_{vJ}^{v'J'})\Big/\sum_{v'''J'''}(\nu_{v'''J'''}^{v'J'})^3 \times q_{v'v'''}\frac{S_{J'''J'}}{(2J'+1)}\right]$$

to obtain the integrated fluorescence intensity. We approximate the preceding expression by

$$\sum_{v}\left[(\nu_{v0}^{v'0})^4 q_{v'v}R(\lambda_{v0}^{v'0})\Big/\sum_{v'''}(\nu_{v'''0}^{v'0})^3 q_{v'v'''}\right]$$

since $\nu_{vJ}^{v'J'}\approx\nu_{v0}^{v'0}$ and $R(\lambda_{vJ}^{v'J'})\approx R(\lambda_{v0}^{v'0})$.

In principle, once the necessary intensity factors (q's and S's) are calculated one should be able to deduce the number density of individual vibrotational states from the above expressions by measuring the fluorescence intensity and laser energy density. In practice, a simulation procedure is necessary to extract reliable relative populations of products from the excitation spectra because of the finite laser bandwidth (0.3–0.4 Å) and the overlapping of six different branches associated with an individual vibrotational state in $^2\Sigma$–$^2\Pi_{1/2 \text{ or } 3/2}$ transitions, or four different branches in $^2\Sigma$–$^2\Sigma$ transitions. A computer program has been written for this purpose. The $^2\Sigma$–$^2\Pi$ transitions were treated in the intermediate case a–b coupling, and the rotational line strengths were taken from Kovac's book.[11] Several approximations have been made to facilitate the analysis: (i) Eq. (1) assumes a constant electronic transition moment, and this approximation is supported by the lifetime measurements made for different vibrational states; (ii) Franck–Condon factors[12] computed for $J'=J''=0$ were used for all J' and J''; (iii) a triangular laser wavelength output has been used for convolution; (iv) in the case of YO two different constant laser bandwidths were used for the X–$\Pi_{1/2}$ (0.45 Å) and X–$\Pi_{3/2}$ (0.35 Å); a single laser bandwidth was used for ScO (the laser band width was measured by using a $\frac{3}{4}$ m spectrometer, or by measuring the broadening of Y atomic lines in the excitation spectra, and the two methods agreed within 20%; (v) a two-parameter functional form

$$P_v(J)=(2J+1)\left[1-(J/J_{\max})^N\right]^M \tag{2}$$

was employed to represent the rotational distribution for all vibrational manifolds of states. In the early simulation of the YO excitation spectra the usual Boltzmann distribution (one parameter) was tried. However, in order to fit the two transitions X–$\Pi_{1/2}$ and X–$\Pi_{3/2}$ we had to use two different rotational temperatures and the difference was as much as 40%–50%. As discussed previously since the two excitation spectra are mainly dominated by different portions of the rotational distribution, we conclude that this one parameter functional form is not flexible enough to yield the true rotational distributions. Figure 9 displays a typical cal-

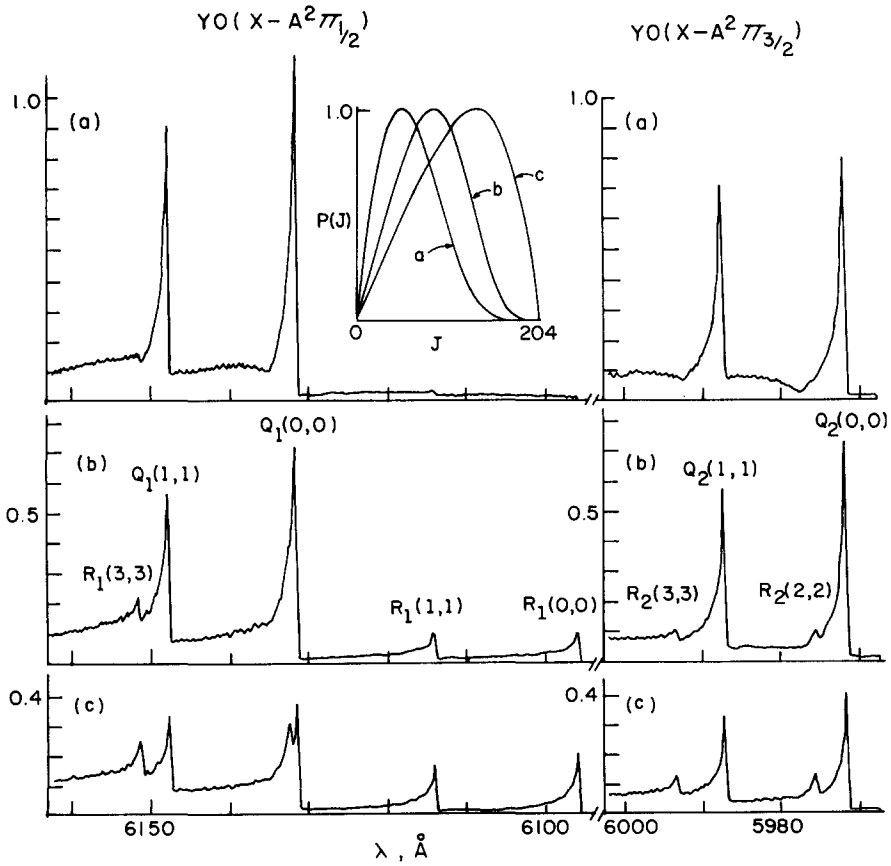

FIG. 9. The dependence of the gross features of excitation spectra on the rotation distribution. All spectra are normalized to the same area with only part of the spectrum shown here.

TABLE II. Spectroscopic constants (cm^{-1}) used in the computer simulation and FC factor calculations.

Molecule	State	T_0	ω_e	$\omega_e x_e$	β_e	α_e	D	
ScO	$X^2\Sigma$	0	971.6	3.95	0.51507	0.0033	5.8×10^{-7}	
	$A^2\Pi_{1/2}$	16440.6	875.0	4.98	0.5042	0.0038	6.1×10^{-7}	-0.0748[a]
	$A^2\Pi_{3/2}$	16554.8	874.6	4.99				
	$B^2\Sigma$	20570.79	825.47	4.21	0.48451	0.0032	6.74×10^{-7}	-0.0665[b]
YO	$X^2\Sigma$	0	862.0	2.86	0.3889	0.0016	3.2×10^{-7}	
	$A^2\Pi_{1/2}$	16315.34[c]	821.36[d]	3.44[c]	0.3866[c]	0.0019	3.5×10^{-7}	-0.151[a]
	$A^2\Pi_{3/2}$	16743.80[c]		3.40[c]				

[a]Λ doubling constant.
[b]Spin splitting constant.
[c]Reference 6(a).
[d]This work (see text).

culation to show the sensitivity of the dependence of parameters (N, M) on the excitation spectra. In Eq. (2) J_{max} depends on the vibrational level and is determined by the energy available to populate that vibrational level, i.e., $J_{max} \cong \sqrt{(E_{total} - E_v)/B_v}$. Note that this form will give the prior distribution in the information-theoretic approach of Levine and co-workers,[13] if $N=2$ and $M=0.5$ for atom + diatomic reaction systems, or $N=2$, $M=2.5$ for two diatomic products. In general, a decrease in N will tend to broaden the distribution, whereas a decrease in M tends to shift the distribution to higher rotational states. We note that Eq. (2) assumes the separation of the vibrational–rotational distribution according to $P(v, J) = P(v)P_v(J)$. Because of uncertainties in the $P_v(J)$ obtained in the fitting procedure, use of more elaborate forms for $P(v, J)$ was not justified. As a check of the program and approximations (i)–(iv) a thermal YO excitation spectrum was measured experimentally (up to $v''=4$) and compared with the calculated spectrum at the same temperature. The agreement was very good.

Although quite a number of spectroscopic studies have been performed on YO and ScO, the constants given in Rosen's compilation[14] gave unsatisfactory fits to the experimental band origin and bandhead positions. Recently, Gole *et al.*[6a] have reanalyzed previous work by others and obtained a new set of spectroscopic constants. Those values indeed improve the simulated spectrum, but differences are still significant. Due to the uncertainty of the absolute laser wavelength (since the wavelength drive is slightly nonlinear over such a wide scan) we did not attempt a major refinement of the spectroscopic constants. Rather, we simply varied the constants for the A state, keeping the ground state constants unchanged, until we matched all the bandhead and band origin positions. Table II lists the constants we used in this work. The best fit rotational distribution parameters (N, M) for the systems studied are listed in Table III, along with some other important

TABLE III. Important parameters in simulated rotational distributions.

Reaction	$J_{max}(v=0)$[a]	$J_{m.p.}(v=0)$	(N, M)
$Y + O_2 \rightarrow YO + O$	221	90	(5, 17.5)
$Y + NO \rightarrow YO + N$	142	105	(1.85, 0.4)
$Y + SO_2 \rightarrow YO + SO$	204	89	(4, 6.5)
$Sc + O_2 \rightarrow ScO + O$	181	58	(3.5, 15)
$Sc + NO \rightarrow SCO + N$	106	75	(2, 0.5)
$Sc + SO_2 \rightarrow ScO + SO$	165	62	(3, 6)

[a]Metal oxide bond strengths from Ref. 14 were used.

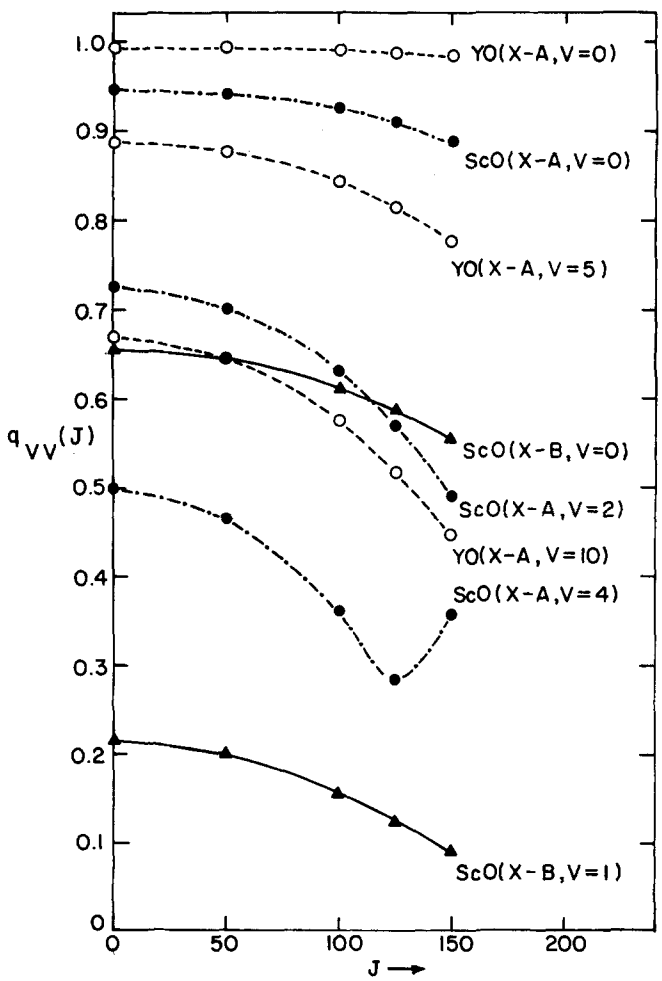

FIG. 10. The rotational state dependence of FC factors for some typical Q branches in $\Delta v = 0$ sequences. Dots represent the calculations from the RKR method and the dash lines show the third-order polynomial fitting (see text).

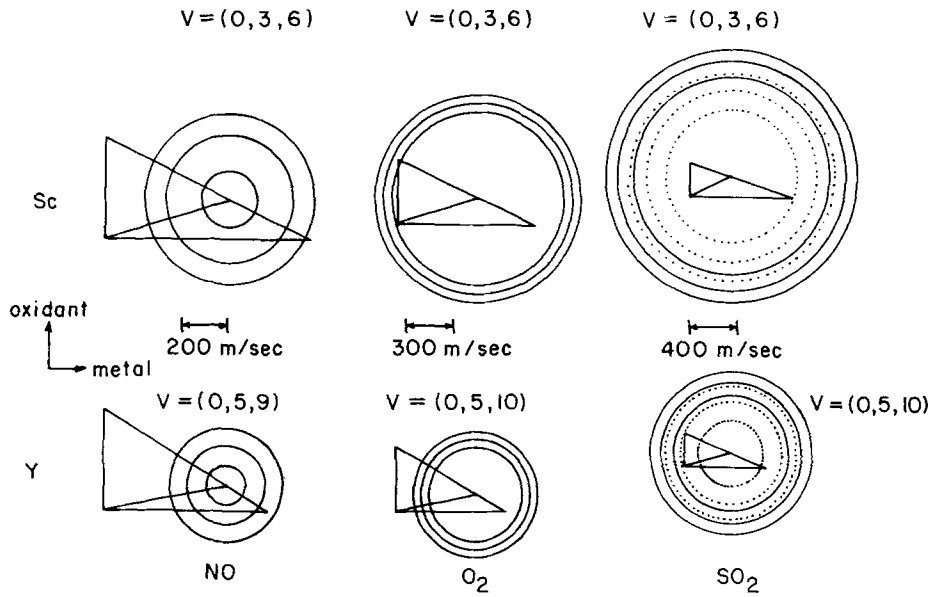

FIG. 11. Simplified Newton diagrams for the reactions studied in this work. The numbers given in parentheses represent the product vibrational state circles calculated for rotationless metal oxides. For the reactions with SO_2 dotted lines indicate the vibrational circles calculated by assuming a prior distribution of energy in the other product fragment (SO), whereas solid lines indicate those obtained by assuming that all of the rest of energy goes into relative translation.

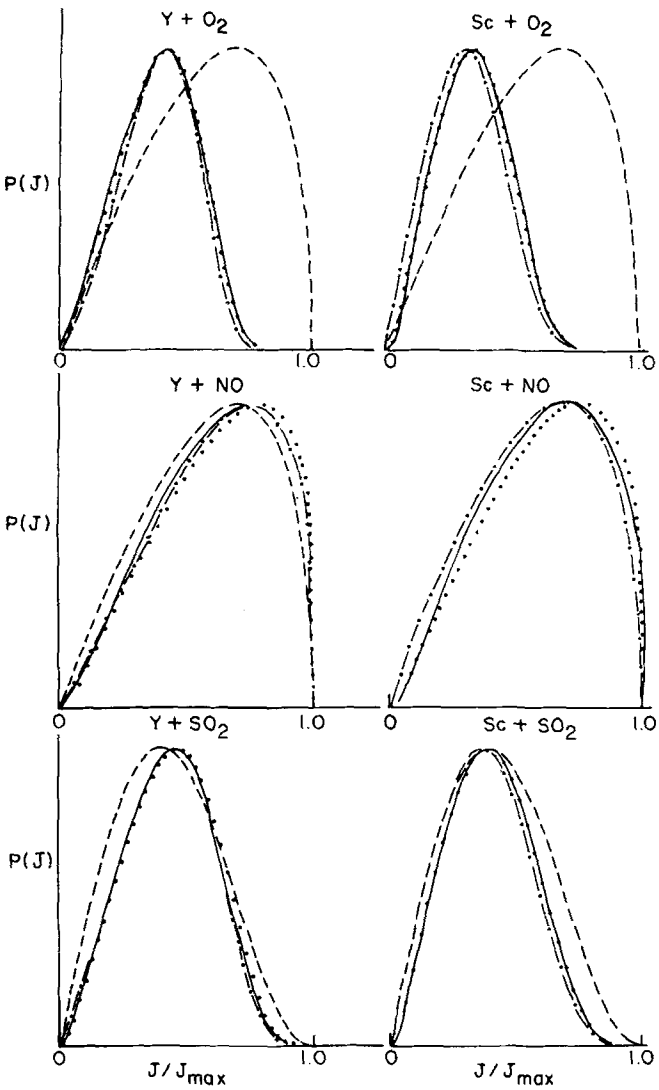

FIG 12. Rotational distribution of metal oxide ($v=0$) for the various reactions. —·—·, experimental number density; —, experimental flux assuming forward scattering; ·····, experimental flux assuming backward scattering; -----, prior calculation.

quantities. The best spectral simulations are shown in Figs. 1–8 above the experimental spectra.

D. Population analysis

To obtain the relative populations of the product internal states several complications have to be considered. Firstly, as mentioned before constant FC factors (i.e., independent of rotational state) have been used. Introduction of the centrifugal term will tend to distort the potential energy curves, and thus cause changes in the FC factors depending on the extent of the distortion. The details of such a calculation have been described extensively by Zare.[12] Figure 10 shows the results for YO, X–A transitions at $J=0$, 50, 100, 125, and 150. As expected the higher the levels (both rotational and vibrational) the more pronounced the change. Since it was impractical to incorporate these variations of the FC factors into the simulation program, we simply used rotationless FC factors in our simulation and corrected the results (both vibrational and rotational distributions) later. Since for any v, J level the FC factors for Q branches usually lay approximately midway between those for P and R branches, and based on the fact that the features of the $^2\Sigma$–$^2\Pi$ spectra are mostly dominated by the Q branches, a third-order polynomial was employed to least-squares fit the Q-branch FC factors for the purpose of this correction.

Secondly, the contribution of thermal YO or ScO originating in the oven had to be removed. This correction was made to the population results rather than to the spectrum itself because it was frequently difficult to obtain good thermal YO or ScO spectra at the same conditions as the reactive YO or ScO spectra.

Thirdly, a correction of product number density to flux density (which is proportional to the detailed rate coefficient[1]) had to be made. Figure 11 shows the Newton diagrams for 90° collisions of the reactants studied, moving at their average velocities. Although single beam experiments were performed, we have

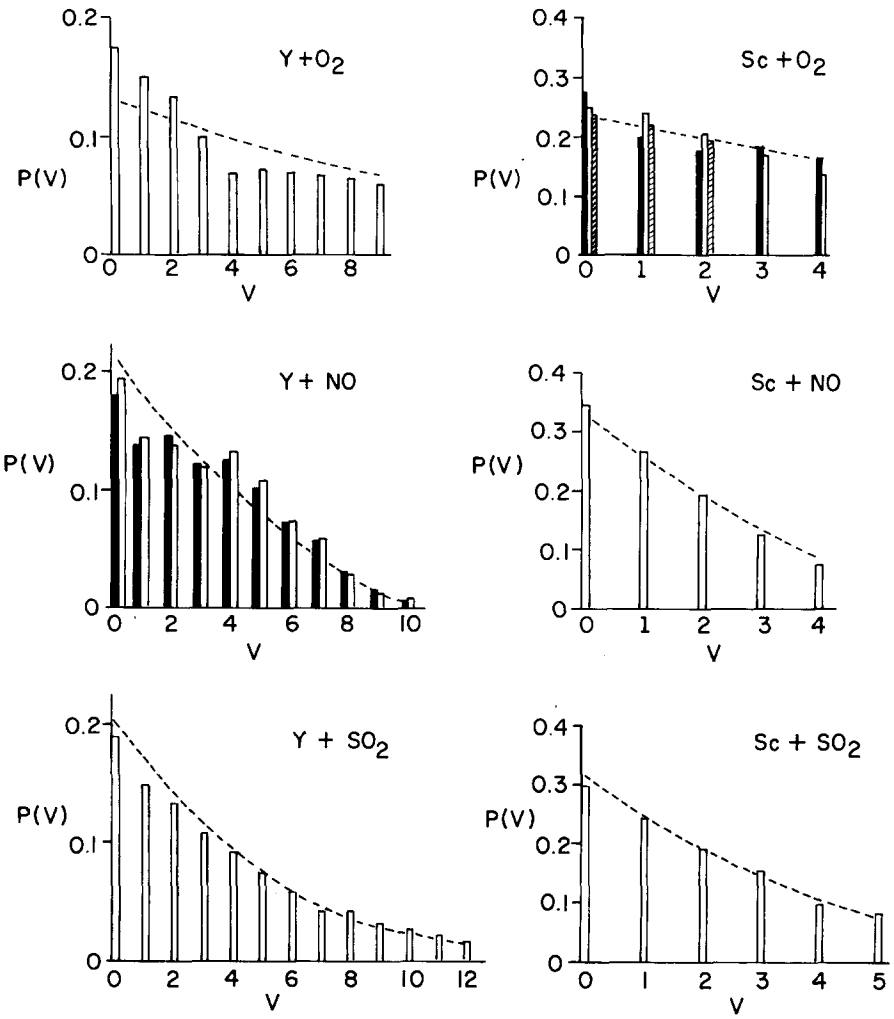

FIG. 13. Vibrational populations of metal oxides for the various reactions. The dot–dashed lines represent the prior distributions. For the reactions of Y + NO and Sc + O_2 the solid bars show the results from the X–$A\ ^2\Pi_{3/2}$ spectrum and empty bars the results from the X–$A\ ^2\Pi_{1/2}$ spectrum. For the Sc + O_2 reaction the slashed bars represent the results from the X–$B\ ^2\Sigma$ spectrum.

considered 90° collisions since they are likely to be representative of the average results when all collision angles are considered. Because of a lack of angular distribution information for these systems, we have considered two extreme cases, forward and backward scattering. For a fixed vibrational level of the product diatomic the laboratory velocity of each individual rotational level was calculated. The relative number density of this state was multiplied by the laboratory velocity to convert it to flux density, and the integrated result for the complete set of rotational levels in this vibrational level gave the relative vibrational flux density. (For the atom + triatomic cases, two calculations were performed: (a) The other diatomic product was assigned a prior distribution of internal energy and (b) the other diatomic product was given no internal energy.) The corrections turned out to have a minor effect on the distributions, as shown in Fig. 12 for the $v = 0$ rotational distribution. The corrected vibrational distributions for the two cases (forward and backward scattering) deviated less than 3% (in opposite directions) from the original number density distribution which is shown in Fig. 13. Although the initial energy spread (which will introduce the necessity for information on the translational energy dependence of the rate coefficients) and collision orientation have not been taken into account, these will affect the distributions markedly only near the energetic limit, which is studied here only for the reaction of Y with NO. Finally, in the case of reaction with O_2 interference from chemiluminescent reactions has to be considered. The ground electronic state can be populated by radiative cascading from excited electronic states. Estimates of relative cross sections for forming ground and excited states described below suggest that corrections for this effect are probably less than uncertainties in the rate coefficients. Taking all of the corrections into account, plus experimental errors, we estimate that the detailed rate coefficients shown in Table IV and Figs. 12 and 13 are accurate within 15%.

E. Energy disposal

Once the product internal state distributions are found it is straightforward to calculate the average energy disposed into various modes. Since we generate $P(v, J)$ by approximating $P(v, J) = P(v)P_v(J)$, the average rotational energy of the product diatomic in a particular vibrational level will be

$$\langle E_R \rangle_v = \int_0^{J_{\max}} E(J) P_v(J) dJ \Big/ \int_0^{J_{\max}} P_v(J)\, dJ.$$

TABLE IV. Relative vibrational populations of MO's deduced from excitation spectra.

Transition analyzed	Y + O_2	Y + NO		Y + SO_2	Sc + O_2			Sc + NO	Sc + SO_2
v	$X-{}^2\Pi$	$X-{}^2\Pi_{1/2}$	$X-{}^2\Pi_{3/2}$	$X-{}^2\Pi$	$X-{}^2\Pi_{1/2}$	$X-{}^2\Pi_{3/2}$	$X-B\,{}^2\Sigma$	$X-{}^2\Pi$	$X-{}^2\Pi$
0	0.174	0.194	0.180	0.191	0.250	0.273	0.364	0.344	0.300
1	0.151	0.143	0.137	0.150	0.239	0.200	0.333	0.265	0.247
3	0.133	0.137	0.144	0.136	0.204	0.180	0.304	0.191	0.190
4	0.0981	0.120	0.121	0.109	0.170	0.182		0.128	0.153
5	0.0663	0.130	0.125	0.0922	0.137	0.165		0.0726	0.105
6	0.0704	0.107	0.102	0.0760					
7	0.0694	0.0729	0.0725	0.0584					
8	0.067	0.0579	0.0575	0.0428					
9	0.064	0.0278	0.0300	0.0430					
10	0.0593	0.0112	0.0140	0.0338					
11				0.0284					
12				0.022					
				0.0174					

Therefore, the average rotational energy of a system can be written as

$$\langle E_R\rangle = \sum_v P(v)\langle E_R\rangle_v \Big/ \sum_v P(v) ,$$

and the average fraction of energy going into rotation is

$$\langle f_R\rangle = \langle E_R\rangle / E_{\text{total}} .$$

The average vibrational energy for a system is

$$\langle E_v\rangle = \sum_v E_v P(v) \Big/ \sum_v P(v) .$$

Similarly, $\langle f_v\rangle = \langle E_v\rangle / E_{\text{total}}$. Due to the large exothermicities for most of the reactions studied and the limited tuning range of the dye laser we were usually unable to observe the spectra up to the energetic limits. In order to compute an "unbiased" experimental result for $\langle f_v\rangle$ we simply extended the observed vibrational populations to the energetic limit using a surprisal analysis based on the observed levels. For the atom + diatomic reactions the fifth column in Table V ($1-\langle f_v\rangle-\langle f_R\rangle$) should give the average fraction of the energy going into product translation, according to the conservation of energy, whereas for the atom + triatomic reactions it will include the internal state excitation of the other product fragment as well.

F. Total reactive cross sections

The relative total cross sections for formation of ground electronic state metal oxides from the different oxidants were obtained by measuring the induced fluorescence intensity at the (0, 0) bandhead. The simulation program was used to convert the ratio of the number of molecules excited at that specific wavelength within the laser bandwidth to a ratio of overall populations of ground electronic state molecules.

Since the same PM tube was also used to monitor the overall chemiluminescence intensity in the case of reaction with O_2, the relative cross sections for production of electronically excited (σ^*) and ground state (σ_g) molecules could be obtained without any absolute calibrations of the detector. To do this several complications had to be taken into account: (i) The photomultiplier tube response differs for the spectral regions in which different products ($A\,{}^2\Pi_{1/2,3/2}$ and $A'\,{}^2\Delta_{3/2,5/2}$)[4,5] radiate; (ii) the use of a short boxcar aperture duration (100 ns) means that only a fraction of the laser excited molecules will radiate in time to be detected; (iii) the LIF measurement yields a population (or number density) which must be converted to a flux for comparison with the chemiluminescence signal by dividing by an average residence time in the excitation zone; (iv) a saturation curve of the type described in the Appendix can be used to determine what fraction of the ground electronic state molecules are excited to fluoresce. By measuring the fluorescent intensity of a laser excited atomic transition (see Appendix) the absolute cross sections could be found as well, since the same detector was used for measuring the product molecules and the metal atom number density. The results of these measurements, listed in Table V, may be uncertain by as much as a factor of 2 or 3, but the relative values for the different gases should be accurate within 20%.

IV. DISCUSSION

A convenient framework for describing the reactions studied here is provided by the information theoretic approach developed by Levine, Bernstein, and coworkers.[13] The method of analyzing energy disposal in this approach is based on the concept of a prior, unbiased distribution. The basic assumption used in deriving the prior distribution is that in the absence of any prior information about the reaction all states of the

TABLE V. Summary of energy disposal and total reactive cross sections.

Reaction	E_{total} (kcal/mole)	$\langle f_v\rangle$	$\langle f_R\rangle$	$1-\langle f_v\rangle-\langle f_R\rangle$	σ_g(Å^2)	σ^*(Å^2)
Y + O_2	55.8	0.27	0.13	0.60	72	2.1
Y + NO	24.9	0.30	0.27	0.43	50	
Y + SO_2	49.8	0.19	0.16	0.65	166	
Sc + O_2	49.7	0.27	0.10	0.63	56	1.5
Sc + NO	18.8	0.23	0.26	0.51	71	
Sc + SO_2	41.8	0.20	0.14	0.66	134	

TABLE VI. Van der Waals constants used in the PST statistical model (see text).

	Y + NO	YO + N	Sc + NO	ScO + N	Y + O_2	YO + O	Sc + O_2	Sc + O
C_6 (10^{-60} erg cm^6)	678	309	554	277	649	223	531	201

products are equally probably as long as they are energetically accessible. Evaluating the prior distribution therefore simply involves counting the number of states of the products at a fixed total energy, followed by an average over the total energy available. No reference need be made as to how the product molecules are formed. The inclusion of conservation laws for quantities other than energy, such as angular momentum, will definitely require more specific information about the reaction process. Hence, it is worthwhile to use the simplest prior distributions in initial comparisons with experiment in order to avoid arbitrary choices which are necessary for imposing additional kinematic or dynamic constraints. In many cases the simplest prior distributions agree well enough with experiment to suggest that these additional constraints play only a minor role.[4,13] These simple prior distributions for product rotational and vibrational states are compared in Figs. 12 and 13 with the experimental distributions. Because of the large exothermicity of the reactions studied, the spread in the initial energy available to the reactants was small compared to the total energy available to the products, and hence a single nominal total energy available could be used in these prior calculations (except for the Y + NO reaction, where averaging was performed to obtain the prior vibrational distribution).

Inspection of Figs. 12 and 13 reveals several interesting results. Firstly, for a given oxidant both the vibrational and rotational distributions of the metal oxide are fairly similar for the case of Y and Sc. Secondly, although the vibrational distributions of metal oxide follow the prior distributions quite well, the agreement does not hold for all of the rotational distributions. The reactions with O_2 are seen to produce considerably less rotational excitation than expected. One might suspect that this deviation is due to a severe limitation of total angular momentum in these reactions. Further, one can ask whether the product rotational distributions are essentially "statistical," but distorted from the prior shape because of the effects of angular momentum conservation.

To answer this question, at least partially, the familiar phase space theory (PST) developed by Light and Pechukas[15] has been applied to the atom–diatom reactions. In the PST it is assumed that this dissociation of the complex depends only on the dynamical quantities (E, J, and M_J) conserved in the reaction and not on the initial reactant states from which the complex is formed. The limitation in orbital angular momentum of products and reactants is obtained from the condition that the translational energy be greater than the centrifugal barrier in the effective two body potential, assumed here to be of the form $-C_6/r^6 + l(l+1)\hbar^2/(2\mu r^2)$. The necessary C_6 constants were approximated by the Slater–Kirkwood method as described previously,[4] and are listed in Table VI. Figure 14 shows the product rotational distributions calculated from this model. The prior distributions are also displayed for comparison. The PST results show a slight shift toward a lower J peak in the distributions, but still predict considerably more rotational excitation than observed in the O_2 reactions. Evidently, inclusion of angular momentum in this manner has only a small effect on the product rotational distributions. The PST vibrational distributions are not shown here, but were similar to the prior curves as has been observed previously.[4] Although calculations of the PST distributions for atom–triatomic reactions were not performed, we expect similar results.

We now ask whether a different statistical theory might give rotational distributions in better agreement with the O_2 results. Most statistical models for indirect reactions rely on two fundamental assumptions: (i) The reaction process can be treated as two separate

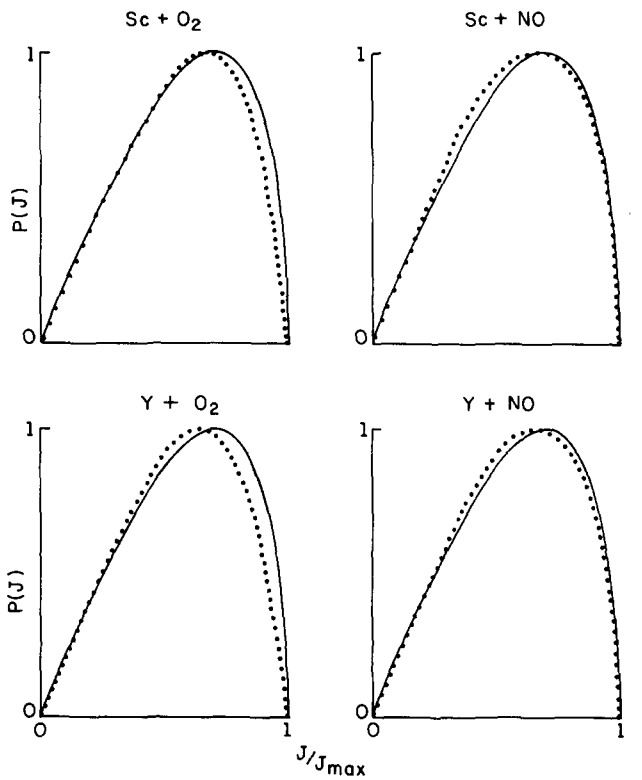

FIG. 14. Rotational distributions from phase space calculations (dotted). The prior distributions (solid) are shown for comparison.

processes, the formation of a complex and the decomposition of the complex with the two being uncorrelated except as dictated by conservation laws and the principle of microscopic reversibility; and (ii) the probabilities of decomposition into various states of the products are taken to be the same. In applying approximation (ii) one selects a certain portion of the state-to-state transition probability matrix, sets the values of all elements in that portion of the matrix equal, and ignors the other elements. In other words, one calculates the "available" product phase space for each product state which is measured. The difference among various statistical models lies mainly in how they constrain that portion of the matrix considered or the available phase space. In constraining the phase space dynamic effects inevitably enter into a statistical theory. For example, in the PST calculation described above a two-body van der Waals interaction controls the particle motion at the critical point where branching into various states occurs. Alternatively, one can parameterize the available phase space using a more realistic potential energy surface as Troe has done,[16] or an even simpler hard sphere criterion as Light and Lin[15a] and Kafri[17] have used for the critical point where branching occurs. We have chosen the Light and Lin approach because very little is known about the potential energy surfaces in these systems. Several parameters are necessary in order to carry out such a calculation: the hard sphere radii for the reactant and product channels and the potential energy at the hard sphere radii. We have taken the potential energy to be zero for the reactant and product channels because there is no reason to expect potential energy barriers in these systems. The reactant channel radius has been estimated to be 4.8 Å for $Y+O_2$ and 4.2 Å for $Sc+O_2$ from the crude approximations to the total cross sections given in the previous section. The product channel radius was taken as an adjustable parameter. Also, the effect of variations in the reactant channel radius about the estimated value was investigated. It proved to be possible to fit the experimental rotational distributions approximately using this statistical model. However, the values of the product channel radius obtained were unreasonably small, coming out even smaller than the metal monoxide bond length. Hence, we can conclude that the reactions of Y and Sc with O_2 appear to give nonstatistical distributions of rotational energy even when angular momentum conservation is taken into account in two rather dissimilar manners. This result then suggests that these reactions are direct, while the reactions with NO and SO_2 proceed via formation of long-lived complexes. Also, in contrast to these results for ground electronic state metal oxides formed in the O_2 reactions are the results of Manos[18] on excited electronic state metal oxides, which indicate that statistical vibrational and rotational distributions are generated. Menzinger and Wren[19] have used an RRK argument to explain how reactions could possibly proceed by long-lived complex mechanisms in forming excited products, but follow direct mechanisms in forming ground state products. Angular distributions of products would be very useful for further clarifying the roles of direct and complex mechanisms in these reactions.

Similar experiments have been performed on the reactions of La with NO, SO_2, and CO_2. Because of severe interference from laser excited La atomic transitions, the results were much less reliable than in the cases of Sc and Y. Nevertheless, we could conclude that the vibrational and rotational distributions are close to prior distributions for all these reactions.

ACKNOWLEDGMENTS

We would like to thank Dr. D. M. Manos and Mr. T. J. Conway for assistance in constructing the apparatus used in these experiments. Computer time was provided by The Ohio State University Computation Center.

APPENDIX: LASER INDUCED FLUORESCENCE EXPERIMENTS UNDER PARTIALLY SATURATED CONDITIONS

Because of weak or noisy fluorescence signals it may be necessary in some LIF experiments to operate under conditions of a partially saturated transition by increasing the laser power. This was the case in our study of the $Sc+O_2$ reaction using excitation of the ScO ($X-A$) transition. Complications arise because the fluorescence intensity is no longer linearly proportional to laser intensity. The following treatment shows how the saturation effect arises, and how to abstract the vibrational population from a partially saturated spectrum.

Comparing the laser pulse period (5–10 ns), the repetition rate ($\leq$200 pps), and the residence time of product molecules in the excitation zone ($<10^{-4}$ s) we note that it will be appropriate to treat the problem as excitation by a single laser pulse. At any time while the laser is on (starting time taken as $t=0$) we have

$$\frac{dn_{ex}}{dt} = (k_{ex} n - k_{de-ex} n_{ex}) I_l - k_{rad} n_{ex} , \tag{A1}$$

where $n_{ex}(t)$ is the concentration of molecules in the excited state, $n(t)$ is the concentration of ground state molecules, I_l is the laser intensity, k_{ex} and k_{de-ex} represent the rate coefficients for the laser excitation and de-excitation (stimulated emission) processes, respectively, and k_{rad} is the rate coefficient for spontaneous emission. Optical pumping by radiation to form some other lower state can be left out in this treatment because of the shortness of the laser pulse compared to the radiative lifetimes involved. Hence, $n_{ex}(t)+n(t)$ will be a constant equal to the initial concentration of ground state molecules N_0. Substituting $n(t)=N_0-n_{ex}(t)$ into Eq. (A1) and approximating I_l as a constant it is readily seen that the population of excited molecules while the laser is on is

$$n_{ex}(t) = \left(\frac{1-e^{-kt}}{k}\right) N_0 k_{ex} I_l , \tag{A2}$$

where $k=(k_{ex}+k_{de-ex})I_l+k_{rad}$. If the laser pulse duration is Δt, then the number of molecules fluorescing within this time is

$$N_1 = \int_0^{\Delta t} n_{ex} k_{rad} dt . \tag{A3}$$

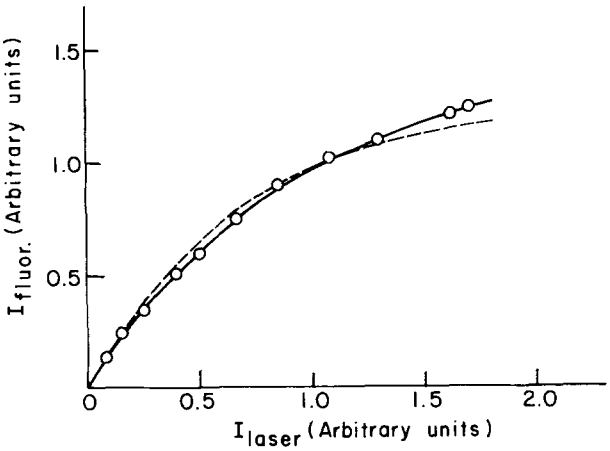

FIG. 15. Saturation curve for the transition ScO (X–$A\,^2\Pi$). The dashed curve represents a calculation based on Eq. (A8). The solid smooth curve through the points was used in correcting for the saturation effect in the vibration population analysis.

Furthermore, if the radiative lifetime of the electronically excited molecule is much shorter than the residence time, then all of the excited molecules will radiate before they fly out of the region viewed by the detector, and the number of molecules fluorescing after the laser pulse can be written as

$$N_2 = n_{ex}(\Delta t)\int_{\Delta t}^{\infty} e^{-(t-\Delta t)k_{rad}} k_{rad}\,dt = n_{ex}(\Delta t). \tag{A4}$$

Substituting the explicit expression (A2) for n_{ex} into Eqs. (A3) and (A4) one obtains the total number of molecules fluorescing spontaneously

$$N = N_1 + N_2 = \frac{N_0 k_{ex} I_l}{k}\left[k_{rad}\Delta t - \frac{k_{rad}}{k} + 1 + \left(\frac{k_{rad}}{k} - 1\right) e^{-k\Delta t}\right]. \tag{A5}$$

k_{ex} and k_{de-ex} used here are the usual Einstein B coefficients and are related to each other by the ratio of degeneracy factors of the two states connecting the transition. For simplicity in the following discussion we take $k_{ex} = k_{de-ex}$ (more general expressions are readily derived): (i) I_l is so small that $k_{rad} \gg k_{ex} I_l$, i.e., most of the excited molecules go back to the ground state by means of spontaneous emission. Then Eq. (A5) becomes

$$N \cong N_0 k_{ex} I_l \Delta t\,, \tag{A6}$$

which has been used in analyzing the unsaturated experiments. (ii) For I_l very large complete saturation occurs, and Eq. (A5) becomes

$$N \cong \tfrac{1}{2} N_0 (k_{rad}\Delta t + 1)\,. \tag{A7}$$

In this case the integrated fluorescence intensity is independent of laser intensity. (iii) If $k_{ex} I_l$ is much larger than k_{rad} but not as large as in case (ii), then partial saturation occurs, and Eq. (A5) becomes

$$N \cong \tfrac{1}{2} N_0 (1 + k_{rad}\Delta t - e^{-2k_{ex} I_l \Delta t})\,. \tag{A8}$$

It is obvious that the integrated fluorescence intensity is no longer proportional to the laser intensity or to k_{ex}. The quantity $2k_{ex} I_l \Delta t$ can be regarded as a "saturation parameter" which is a measure of the degree of saturation. In order to obtain population information using Eq. (A8) we must first be able to calculate the values for k_{rad} and k_{ex}. Although this is straightforward in the atomic case, the situation becomes more complicated for molecular transitions. Furthermore, the measurement of the absolute laser intensity will impose another source of error. In view of these difficulties we feel that an experimental method for determining the saturation parameter is more appropriate. A series of relative laser intensities (I_l') and their corresponding relative integrated fluorescence intensities (N') for a particular transition are measured. A plot of N' vs I_l', as shown in Fig. 15, will be called a saturation curve. If k_{rad} is known from lifetime measurements, then we can readily obtain a value for k_{ex}' by varying it until we fit the experimental curve $\ln N'$ vs I_l' to the form $\ln(1 + k_{rad}\Delta t - e^{-2k'_{ex} I_l' \Delta t})$. Then k_{ex}' and I_l' are substituted into Eq. (A8) to find N'/N_0', the fraction of molecules which are induced to fluoresce spontaneously when the laser power is I_l'. Two atomic lines Y(6191.7 Å) and Sc (6210.7 Å) were chosen to test this method. In the case of Y an experimental saturation parameter of 1.75 was obtained compared to a calculated value of 2.6, and for Sc an experimental value of 1.45 compared to a calculated value of 1.5 (degeneracy factors being incorporated in the calculations). When application is made to a molecular transition, e.g., the ScO(X–A) excitation spectrum for the $Sc + O_2$ reaction shown in Fig. 16, one more approximation is made, namely, the

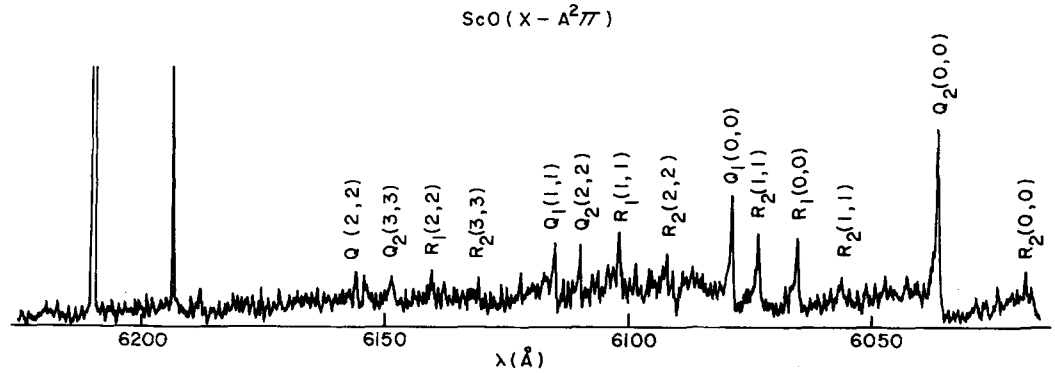

FIG. 16. ScO excitation spectra of the $X\,^2\Sigma^+$–$A^2\Pi$ transition for the $Sc + O_2$ reaction under partially saturated conditions.

saturation curve is assumed to be the same for different bands if the axis for I_t' is scaled by the corresponding FC factor to correct for different values of k_{ex}. (Since we were only concerned with extracting relative vibrational populations from these spectra, no correction was made for the dependence of k_{ex} on rotational state.) The results of the vibrational population analysis based on use of a saturation curve are shown in Fig. 13 and included in Table IV. Relative peak areas were used to obtain these results. The relative populations are in good agreement with those used to simulate the unsaturated X–B excitation spectrum.

We note that the treatment in this Appendix does not take into account polarization effects. Since the output of the dye laser is polarized (to a varying extent for different dyes), one might expect some effect on the degree of saturation. Similar formulations have been developed to include this effect, and calculations were performed for the atomic transitions Y (6191.7 Å) and Sc (6210.7 Å). The results for N/N_0 were within 5% of the values obtained by the simple Eq. (A8) and hence corrections of the molecular transitions were not attempted.

[1]H. W. Cruse, P. J. Dagdigian, and R. N. Zare, Discuss. Faraday Soc. **53**, 277 (1973).
[2]R. N. Zare and P. J. Dagdigian, Science **185**, 739 (1974).
[3](a) J. L. Kinsey, J. Chem. Phys. **66**, 2560 (1977); (b) M. H. Alexander, P. J. Dagdigian, and A. E. Depristo, J. Chem. Phys. **66**, 59 (1977); (c) W. Schmidt, A. Siegel, and A. Schultz, Chem. Phys. **16**, 161 (1976); (d) P. J. Dagdigian, H. W. Cruse, A. Schultz, and R. N. Zare, J. Chem. Phys. **61**, 4450 (1974); (e) J. G. Pruett, and R. N. Zare, J. Chem. Phys. **62**, 2050 (1975); (f) J. G. Pruett and R. N. Zare, J. Chem. Phys. **64**, 1774 (1976); (g) G. P. Smith and R. N. Zare, J. Chem. Phys. **64**, 2632 (1976); (h) R. K. Sander, B. Soep, and R. N. Zare, J. Chem. Phys. **64**, 1242 (1976).
[4]D. M. Manos and J. M. Parson, J. Chem. Phys. **63**, 3575 (1975).
[5]C. L. Chalek and J. L. Gole, J. Chem. Phys. **65**, 2845 (1976).
[6](a) C. L. Chalek and J. L. Gole, Chem. Phys. **19**, 59 (1977); (b) D. R. Preuss and J. L. Gole, J. Chem. Phys. **66**, 2994, 3000 (1977).
[7]*Metals, Thermal and Mechanical Data: International Tables of Selected Constants*, edited by S. Allard (Pergamon, Oxford, 1969), Vol. 16.
[8]T. W. Hansch, Appl. Opt. **11**, 895 (1972).
[9]P. J. Dagdigian, H. W. Cruse, and R. N. Zare, J. Chem. Phys. **60**, 2330 (1974).
[10]The assignment of bandheads is according to A. Gatterer, J. Jenkes, and E. W. Salpeter, *Molecular Spectra of Metallic Oxides* (Specola Vaticana, Vatican City, 1958).
[11]I. Kovacs, *Rotational Structure in the Spectra of Diatomic Molecules* (American Elsevier, New York, 1969).
[12]R. N. Zare, J. Chem. Phys. **40**, 1934 (1964).
[13](a) R. D. Levine and R. B. Bernstein, Discuss. Faraday Soc. **53**, 100 (1973); (b) R. B. Bernstein and R. D. Levine, Adv. At. Mol. Phys. **11**, 215 (1975); (c) R. D. Levine and A. Ben-Shaul, *Chemical and Biochemical Applications of Lasers*, edited by C. B. Moore (Academic, New York, 1977).
[14]*Spectroscopic Data Relative to Diatomic Molecules: International Tables of Selected Constants*, edited by B. Rosen (Pergamon, Oxford, 1970), Vol. 17.
[15](a) P. Pechukas and J. C. Light, J. Chem. Phys. **42**, 3281 (1965); (b) P. Pechukas, J. C. Light, and C. Rankin, J. Chem. Phys. **44**, 794 (1966); (c) J. Lin and J. C. Light, J. Chem. Phys. **45**, 2545 (1966).
[16]M. Quack and J. Troe, Ber. Bunsenges. Phys. Chem. **80**, 1140 (1976) and references cited therein.
[17]A. Kafri, Chem. Phys. **13**, 309 (1976).
[18]D. M. Manos, Ph.D. Thesis, The Ohio State University, 1976.
[19]M. Menzinger and D. J. Wren, Chem. Phys. Lett. **18**, 431 (1973).